Materials Transactions, JIM, Vol. 41, No. 10 (2000) pp. 1329 to 1336

Phase Equilibria in Nb–Mo-Rich Zone of the Nb–Si–Mo Ternary System

Chao-Li Ma[1], Yi Tan[1], Hisao Tanaka[1], Aoki Kasama[1], Ryohei Tanaka[1], Seiji Miura[2], Yosinao Mishima[3] and Shuji Hanada[4]

[1]*Japan Ultra-high Temperature Materials Research Institute, Ube 755-0001, Japan*
[2]*Graduate School of Engineering, Hokkaido University, Sapporo 060-8628, Japan*
[3]*Department of Materials Science and Engineering, Tokyo Institute of Technology, Yokohama 226-8502, Japan*
[4]*Institute for Materials Research, Tohoku University, Sendai 980-8577, Japan*

Microstructures and phase equilibria in cast and annealed Nb–Mo–Si alloys near the Nb–Mo binary were studied using X-ray diffraction (XRD) analysis, scanning electron microscopy (SEM), and electron beam microprobe analysis (EPMA). A broad range of Nb and Mo compositions were investigated for Si compositions up to 30 mol%. Microstructural and microchemical evidence provide a clear definition of the Nb–Mo–Si liquidus surface projection and an isothermal section diagram at 1973 K.

(Received February 16, 2000; Accepted September 5, 2000)

Keywords: *liquidus surface projection, isothermal section, phase equilibria, microstructure, phase diagram, niobium-molybdenum-silicon ternary system, in-situ composite*

1. Introduction

In-situ composites based on Nb–Si alloys are potential structural materials for use at elevated temperature.[1–4] To achieve good balance of high-temperature strength and room-temperature toughness, microstructure control and phase chemistry optimization are the most important issues in developing this kind of material.[4] Alloying study has revealed that Mo and/or W additions to Nb alloys remarkably increase their high-temperature strength, but diminish their deformability at room temperature.[5] In our recent studies,[6] it was found that Mo and/or W addition to Nb/Nb-silicide *in-situ* composite produced by arc-melting improves its low-temperature deformability as well as high temperature strength. To understand these phenomena, the knowledge of microstructure evolution associated with phase relationship and microstructural formation of these ternary alloys is necessary. Unfortunately, few data are available to meet such demands at present.[7,8] The purpose of this paper is to study the phase relationships and equilibria in the ternary Nb–Mo–Si system. Based on the results of microstructural and microchemical analyses performed on the cast and the heat-treated alloys with Nb–Mo-rich compositions, liquidus surface projection and isothermal section diagram at 1973 K are proposed.

2. Background on the Nb–Mo–Si Ternary Equilibria

In this paper, the Nb–Mo-rich zone (up to 37.5%Si; all compositions are given in mol percent through the paper, unless otherwise stated) of the ternary Nb–Mo–Si system is considered. In this area, the binary Nb–Si phase diagram[9] possesses two liquid-solid transformations of (1) eutectic reaction, L $\rightarrow$ $Nb_3Si + Nb_{ss}$ at 2193 K for 18.7%Si; and (2) peritectic reaction, L + β-Nb_5Si_3 $\rightarrow$ Nb_3Si at 2253 K for 19.5%Si. Similarly, in the binary Mo–Si phase diagram[9] there are also two liquid-solid reactions of (1) eutectic reaction, L $\rightarrow$ $Mo_3Si + Mo_5Si_3$ at 2297 K for 26.4%Si; and (2) peritectic reaction, L + Mo_{ss} $\rightarrow$ Mo_3Si at 2298 K for 25.72%Si. In binary Nb–Mo phase diagram,[9] there is a continuous solid solution between Nb and Mo. On the basis of these three binary phase diagrams, a possible Nb–Mo–Si liquidus surface projection is proposed in Fig. 1. To facilitate description of this diagram, in this paper, the Nb in solid solution with Mo and Si is referred to as Nb_{ss}; the Nb_3Si with Mo in solid solution, $(Nb(Mo))_3Si$; the Mo_3Si with Nb in solid solution, $(Mo(Nb))_3Si$; the α-Nb_5Si_3 with Mo in solid solution, α-$(Nb(Mo))_5Si_3$. Because β-Nb_5Si_3 and Mo_5Si_3 are isomorphous, the β-Nb_5Si_3 with Mo, or Mo_5Si_3 with Nb, in solid solution is referred to as β-$(Nb,Mo)_5Si_3$.

As the figure suggests, the partial liquidus surface projection is divided into four regions, where Nb_{ss}, $(Nb(Mo))_3Si$, β-$(Nb,Mo)_5Si_3$, and $(Mo(Nb))_3Si$ appear as a primary phase from the melt, respectively, by several eutectic grooves and peritectic ridges. The β-Nb_5Si_3 forms a continuous solid solution, β-$(Nb,Mo)_5Si_3$, with Mo_5Si_3 from Nb–Si side to Mo–Si side. Between the two binary eutectics of Nb–Nb_3Si (e_2) and Mo_3Si–Mo_5Si_3 (e_1), there is a eutectic groove, which falls in temperature from 2297 K at e_1 to 2193 K at e_2 and intersects with two peritectic ridges from two binary peritectic p_1 and p_2. At the intersection (denoted by U_1) between the eutectic groove that descends from eutectic e_1, and the peritectic ridge from peritectic p_1, the first transition reaction takes place. This reaction is described by:

$$L + (Mo(Nb))_3Si \rightarrow \beta\text{-}(Nb,Mo)_5Si_3 + Nb_{ss}$$

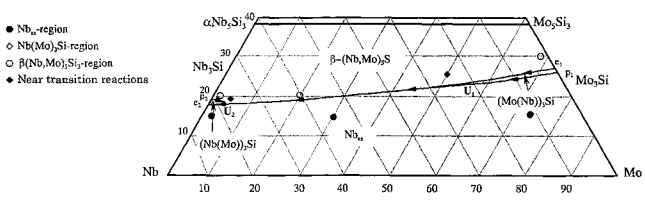

Fig. 1 The proposed liquidus surface projection of Nb–Mo-rich zone of the Nb–Mo–Si ternary system. The various marks in this diagram represent the alloy compositions investigated in this study.

At the intersection (denoted by U_2) between the eutectic groove that descends from the first transition reaction and the peritectic ridge from peritectic P_2, the second transition reaction occurs:

$$L + \beta\text{-}(Nb,Mo)_5Si_3 \rightarrow (Nb(Mo))_3Si + Nb_{ss}$$

3. Experimental Procedure

The investigated compositions are listed in Table 1. The staring raw materials were 99.9 mass%Nb, 99.9 mass%Mo and 99.999 mass%Si elemental powders. Button ingots, each about 20 g, were prepared by non-consumable arc-melting in a water-cooling copper crucible under an ultra high-purity argon atmosphere. Alloy ingots were remelted three times to ensure chemical homogeneity. The mass losses were measured to be less than 0.1 mass% for each ingot after melting, suggesting that the alloy compositions were close to the nominal. Samples for heat treatment were cut using an electro-discharge machine (EDM) and annealed at 1973 K for 48 h, followed by furnace cooling to room temperature.

Microstructural observations were conducted using second electron microscope (SEM). The phases and compositions were determined using X-ray diffraction (XRD) and electron probe microanalysis (EPMA). High-purity Nb (99.99 mass%), Si (99.9999 mass%) and Mo (99.97 mass%) were used as standards and conventional matrix corrections (ZAF) were used to calculate the compositions from the measured X-ray intensities.

4. Results and Discussion

4.1 Liquidus surface

In this section, the microstructural evidence for solidification paths will be described for compositions in each primary phase region, and for compositions near the two transition reactions. It must be indicated here that the actual solidification path might deviate from the equilibrium solidification process, because in our experiments, the melt solidified in a water-cooling copper crucible, which resulted in a relatively high cooling rate. The phases present in the cast alloys are summarized in Table 1.

4.1.1 Nb_{ss}-region

This primary Nb_{ss} phase region covers the Nb_{ss}-rich side of $(Nb(Mo))_3Si$–Nb_{ss} eutectic, β-$(Nb, Mo)_5Si_3$–Nb_{ss} eutectic, and $L + Nb_{ss} \rightarrow (Mo(Nb))_3Si$ peritectic valleys, as shown in Fig. 1.

Figure 2(a) shows a typical back-scattering electron image

Table 1 Alloy compositions and constituent phases of Nb–Mo–Si alloys.

Region	Composition	Phase in As-Cast Condition
Nb_{ss}-region	Nb–16Si–1Mo Nb–16Si–2Mo	Primary Nb_{ss} dendrites, $(Nb(Mo))_3Si$–Nb_{ss} eutectic
	Nb–16Si–4Mo Nb–16Si–5Mo Nb–16Si–10Mo Nb–16Si–15Mo Nb–16Si–20Mo Nb–16Si–30Mo Nb–16Si–40Mo	Primary Nb_{ss} dendrites, β-$(Nb, Mo)_5Si_3$–Nb_{ss} eutectic
	Nb–16Si–74Mo Nb–16Si–83Mo	Primary Nb_{ss} dendrites, Peritectic $(Mo(Nb))_3Si$
$Nb(Mo)_3Si$-region	Nb-19Si-1Mo Nb-19Si-2Mo	Primary $(Nb(Mo))_3Si$ dendrites, $(Nb(Mo))_3Si$–Nb_{ss} eutectic
β-$(Nb, Mo)_5Si_3$-region	Nb–20Si–1Mo	Primary β-$(Nb, Mo)_5Si_3$ dendrites, Peritectic $(Nb(Mo))_3Si$, $(Nb(Mo))_3Si$–Nb_{ss} eutectic
	Nb–19Si–4Mo Nb–20Si–3Mo Nb–25Si–10Mo Nb–25Si–30Mo	Primary β-$(Nb, Mo)_5Si_3$ dendrites, β-$(Nb, Mo)_5Si_3$–Nb_{ss} eutectic
	Nb–30Si–69Mo	Primary β-$(Mo, Nb)_5Si_3$ dendrites, $(Mo(Nb))_3Si$–β-$(Mo, Nb)_5Si_3$ eutectic
Near transition reaction region	First transition reaction: Nb–25Si–50Mo	Primary β-$(Mo, Nb)_5Si_3$ dendrites, $(Mo(Nb))_3Si$–β-$(Mo, Nb)_5Si_3$ eutectic β-$(Nb, Mo)_5Si_3$–Nb_{ss} eutectic
	Second transition reaction: Nb–19Si–3Mo	Primary β-$(Nb, Mo)_5Si_3$ dendrites, β-$(Nb, Mo)_5Si_3$-Nb_{ss} eutectic, $(Nb(Mo))_3Si$–Nb_{ss} eutectic

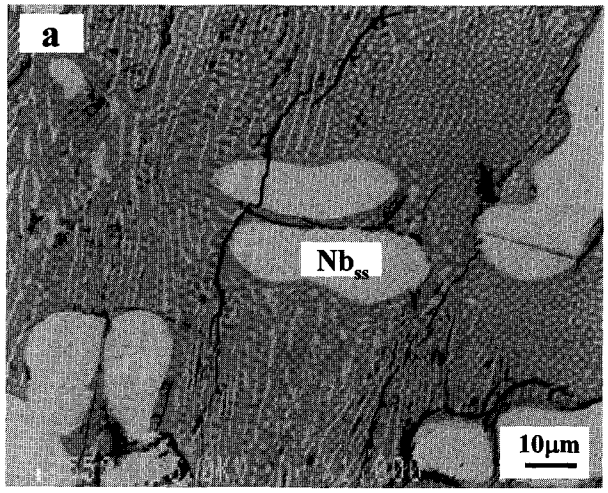

(a)

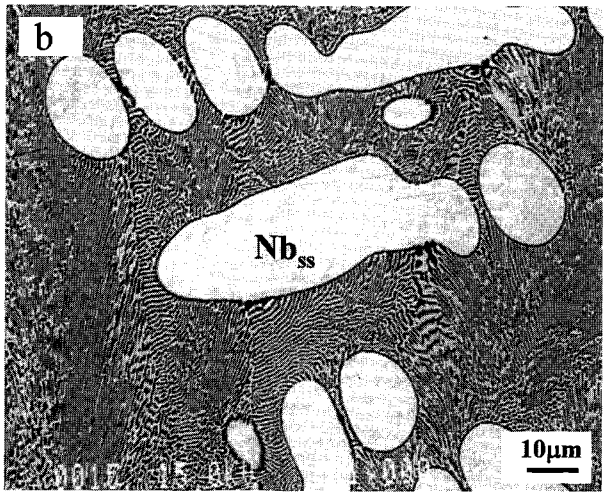

(b)

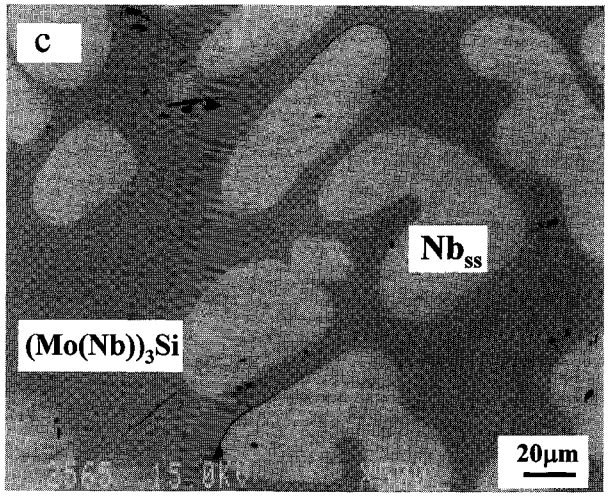

(c)

Fig. 2 BEI micrographs showing typical microstructures of compositions lying on Nb_{ss}-rich side of (a) $(Nb(Mo))_3Si$–Nb_{ss} eutectic reaction valley (Nb–16Si–2Mo), (b) β-$(Nb,Mo)_5Si_3$–Nb_{ss} eutectic reaction valley (Nb–16Si–30Mo), and (c) $L + Nb_{ss} \rightarrow (Mo(Nb))_3Si$ peritectic reaction valley (Nb–16Si–74Mo).

(BEI) of the as cast Nb–16Si–2Mo alloy. The microstructure consists of large, bright, nonfaceted dendritic particles together with a two-phase mixture produced by a eutectic reaction. The dendritic particles were identified using EPMA and XRD to be Nb_{ss} with a mean composition of Nb–3.4Si–2.7Mo. The two-phase eutectic contains very fine light needles or rods in a gray continuous matrix. EPMA result showed a composition of Nb–25.1Si–0.6Mo for the gray continuous phase. The Si concentration is essentially the stoichiometric composition of a Nb_3Si-type phase. X-ray diffraction data confirmed the presence of a Nb_3Si-type phase. Thus, the gray continuous phase is believed to be Nb_3Si with Mo in solid solution, *i.e.*, $(Nb(Mo))_3Si$. The light needles or rods in the eutectic are Nb_{ss}. Therefore, the solidification reaction sequences of Nb–16Si–2Mo alloy can be described as: $L \rightarrow Nb_{ss} + L_1$, then $L \rightarrow Nb_{ss} + (Nb(Mo))_3Si$. The eutectic Nb_{ss}–$(Nb(Mo))_3Si$ is of a similar morphology to the eutectic in cast Nb–16Si alloy,[10,11] suggesting a weak effect on eutectic of the small Mo additions. Some cracks were observed, which was probably due to the different thermal contraction during solidification and the post solidification cooling.

Figure 2(b) shows the BEI micrograph of the as cast Nb–16Si–30Mo alloy. This microstructure possesses large nonfaceted primary Nb_{ss} dendrites and interdendritic eutectic matrix. It is very interesting to note that this eutectic is of very fine lamellar morphology. In the lamellar eutectic areas, the dark phase was β-$(Nb,Mo)_5Si_3$ and the bright lamellas were Nb_{ss}, confirmed by EPMA and XRD analyses. Thus, the eutectic reaction is described as β-$(Nb,Mo)_5Si_3 + Nb_{ss}$. Considering that no responding reaction exists in either Nb–Si system[9] or Nb–Ti–Si[12] system, it is suggested that sufficient amount of Mo addition changes the phase separation behavior during solidification. This feature is useful to produce Nb/Nb silicide *in-situ* composite with a lamellar structure. Table 1 indicates the existence of the eutectic reaction in a very wide Mo composition range from lower than 4% to higher than 40%.

Figure 2(c) shows the cast microstructure of Nb–16Si–74Mo alloy. This composition was investigated to examine the peritectic reaction of $L + Nb_{ss} \rightarrow (Mo(Nb))_3Si$. This microstructure composed of large nonfaceted primary Nb_{ss} particles and a $(Mo(Nb))_3Si$ matrix. Nb_{ss} phase is bright and the $(Mo(Nb))_3Si$ phase is gray in the BEI micrograph. The mean compositions of Nb_{ss} and $(Mo(Nb))_3Si$ were measured to be Nb–5.2Si–87.3Mo and Nb–25.0Si–62.8Mo, respectively. The Si concentration of $(Mo(Nb))_3Si$ is essentially the stoichiometric composition.

This microstructure suggests that the alloy composition locates on the Nb_{ss}-rich side of $(Mo(Nb))_3Si$ peritectic valley. Thus the solidification began with the formation of primary Nb_{ss} dendrites. As solidification proceeded, the liquid composition shifted to the peritectic ridge and met it. This consequently led to the formation of $(Mo(Nb))_3Si$ on the surface of the primary Nb_{ss} particles *via* a peritectic reaction, *i.e.*, $L + Nb_{ss} \rightarrow (Mo(Nb))_3Si$. At this point, there are two possible choices for the cooling path: one is that the melt's composition moves along the peritectic ridge till finishing this solidification process; the other is that the liquid only moves along the peritectic ridge for a short distance, and then shifts off the

peritectic ridge into the adjacent primary $(Mo(Nb))_3Si$ phase region. This led to continuous formation of the $(Mo(Nb))_3Si$ phase. Considering a rapid cooling rate in the arc melting process, the second cooling path is very possible.

4.1.2 β-$(Nb, Mo)_5Si_3$-region

The primary β-$(Nb, Mo)_5Si_3$ phase region covers the β-$(Nb, Mo)_5Si_3$-rich side of L + β-$(Nb, Mo)_5Si_3$ → $(Nb(Mo))_3Si$ peritectic reaction, β-$(Nb, Mo)_5Si_3$–Nb_{ss} eutectic reaction, and β-$(Nb, Mo)_5Si_3$–$(Mo(Nb))_3Si$ eutectic valleys.

Nb–20Si–1Mo: The peritectic reaction of L + β-$(Nb, Mo)_5Si_3$ → $(Nb(Mo))_3Si$ was confirmed by the microstructural observation of Nb–20Si–1Mo alloy. A typical BEI micrograph of this alloy is illustrated in Fig. 3(a), in which some distinct dark particles locate at center areas of large nonfaceted gray dendrites. This is a typical peritectic-type morphology. The dark particles were identified using EPMA and XRD to be β-$(Nb, Mo)_5Si_3$, whilst the large gray dendrites were identified to be $(Nb(Mo))_3Si$. This suggests a peritectic reaction of L + β-$(Nb,Mo)_5Si_3$ → $(Nb(Mo))_3Si$. In the interdendritic area is the eutectic of $(Nb(Mo))_3Si$–Nb_{ss}. The eutectic typically consists of fine-scale Nb_{ss} rods in a $(Nb(Mo))_3Si$ matrix, which is analogous to that observed in Nb–16Si–2Mo, as shown in Fig. 2(a). A few small single $(Nb(Mo))_3Si$ phase particles are occasionally observed in the eutectic matrix (this feature is not included in the present figure).

This microstructure suggests that the composition of Nb–20Si–1Mo is hyperperitectic and close to the L + β-$(Nb, Mo)_5Si_3$ → $(Nb(Mo))_3Si$ peritectic ridge. Upon solidification, the β-$(Nb, Mo)_5Si_3$ phase nucleated and grew in dendritic form within the liquid. The liquid composition shifted to the peritectic ridge and met it. This led to solidification of peritectic $(Nb(Mo))_3Si$ at the surface of primary β-$(Nb, Mo)_5Si_3$ dendrites. However, the liquid composition only followed the peritectic ridge for a short distance, and it dropped off this ridge into the lower primary $(Nb(Mo))_3Si$ phase region. This led to the solidification of $(Nb(Mo))_3Si$ phase. The presence of a few single $(Nb(Mo))_3Si$ phase particles in eutectic matrix may be the evidence of this reaction. The liquid composition continued to move down the $(Nb(Mo))_3Si$-rich region and met the eutectic Nb_{ss}–$(Nb(Mo))_3Si$ groove. This led to solidification of eutectic Nb_{ss}–$(Nb(Mo))_3Si$.

Nb–25Si–30Mo: Figure 3(b) illustrates a typical BEI micrograph of Nb–25Si–30Mo alloy. It is hypereutectic giving rise to primary β-$(Nb, Mo)_5Si_3$ dendrites and Nb_{ss}–β-$(Nb, Mo)_5Si_3$ eutectic matrix. The eutectic shows lamellar morphology, which is similar to that in Nb–16Si–30Mo alloy (see Fig. 2(b)). The primary β-$(Nb, Mo)_5Si_3$ phase, which is dark in the BEI micrograph, shows predominantly nonfaceted dendritic particles. In some regions, especially at the bottom area of the ingot, small angular block-shaped β-$(Nb, Mo)_5Si_3$ are always observed. The factors affecting the morphology of primary β-$(Nb, Mo)_5Si_3$ is not clear at present. The fast cooling rate may be favorable to forming the angular-shaped β-$(Nb, Mo)_5Si_3$ particles, because angular block-shaped β-$(Nb, Mo)_5Si_3$ are always observed at the bottom area, where the cooling rate is relative higher than in the upper region.

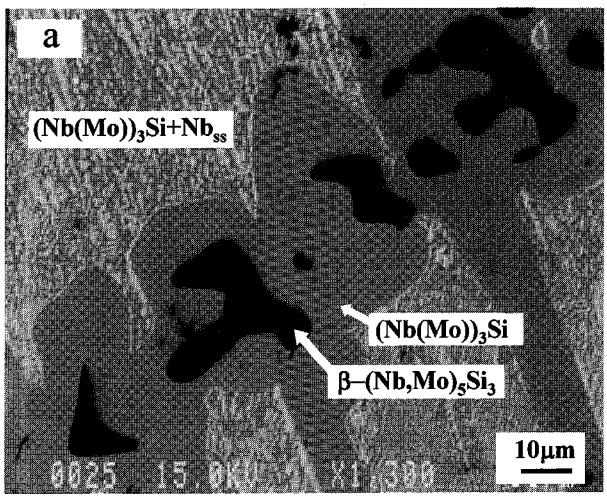

(a)

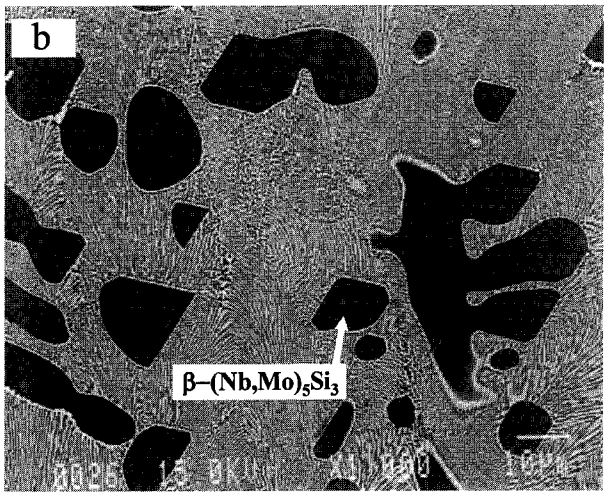

(b)

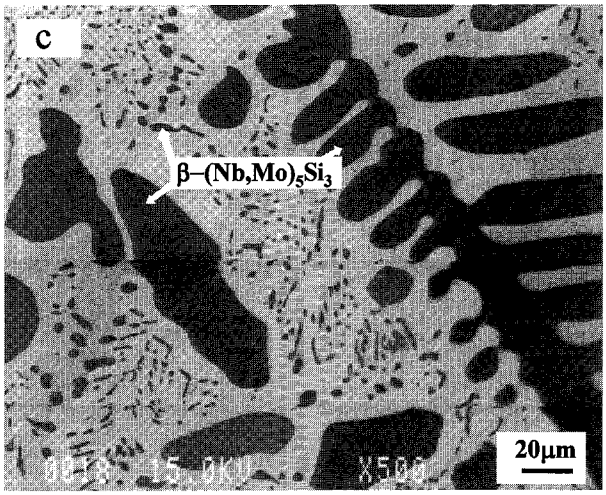

(c)

Fig. 3 BEI micrographs for compositions lying on β-$(Nb, Mo)_5Si_3$-rich side, showing typical microstructures of (a) L + β-$(Nb, Mo)_5Si_3$ → $(Nb(Mo))_3Si$ peritectic reaction (Nb–20Si–1Mo), (b) $(Nb(Mo))_5Si_3$–Nb_{ss} eutectic reaction (Nb–20Si–30Mo), and (c) β-$(Nb, Mo)_5Si_3$–$(Mo(Nb))_3Si$ eutectic reaction valley (Nb–30Si–69Mo).

Compositions of Nb–20Si–3Mo and Nb–20Si–10Mo were also examined in this study, and the microstructures observed were similar to that shown in Fig. 3(b).

Nb–30Si–69Mo: This composition was investigated to examine the eutectic reaction of L → β-$(Nb,Mo)_5Si_3$ + $(Mo(Nb))_3Si$. The microstructure of this alloy in the as cast condition is shown in Fig. 3(c). It consists of primary β-$(Nb,Mo)_5Si_3$ dendrites and β-$(Nb,Mo)_5Si_3$–$(Mo(Nb))_3Si$ eutectic. The β-$(Nb,Mo)_5Si_3$ phase is distinguished by its morphology, composition, and dark contrast in BEI micrograph. The eutectic of β-$(Nb,Mo)_5Si_3$–$(Mo(Nb))_3Si$ consists of small dot-shaped or fine needle-shaped β-$(Nb,Mo)_5Si_3$ particles distributing randomly in $(Mo(Nb))_3Si$ matrix, which is write in BEI micrograph. The mean composition of the primary β-$(Nb,Mo)_5Si_3$ phase is Nb–38.7Si–60.4Mo and the mean composition of $(Mo(Nb))_3Si$ is Nb–25.6Si–73.8Mo.

4.1.3 $(Nb(Mo))_3Si$-region

In the binary Nb–Si phase diagram,[9] the primary Nb_3Si phase exists in a narrow Si content range from 18.7 to 19.5%. It is similar in the ternary Nb–Mo–Si diagram. The primary $(Nb(Mo))_3Si$ phase region lies between the L + β-$(Nb,Mo)_5Si_3$ → $(Nb(Mo))_3Si$ peritectic ridge and the Nb_{ss}-$(Nb(Mo))_3Si$ eutectic groove. As described above, the Nb–16Si–2Mo alloy is hypoeutectic (see Fig. 2(a)), while the Nb–20Si–1Mo alloy is hyperperitectic (see Fig. 3(a)). This gives evidence for the narrow $Nb(Mo)_3Si$-region between the $(Nb(Mo))_3Si$–Nb_{ss} eutectic groove and L + β-$(Nb,Mo)_5Si_3$ → $(Nb(Mo))_3Si$ peritectic ridge.

Ternary Nb–Mo–Si alloys with Si content of 19% and Mo contents from 1 to 3% were investigated to examine the primary $(Nb(Mo))_3Si$ phase and to simply determine the Mo composition range in the $(Nb(Mo))_3Si$-rich region. XRD and microstructural observations showed that both the Nb–19Si–1Mo and Nb–19Si–2Mo contained two phases of Nb_{ss} and $(Nb(Mo))_3Si$. The $(Nb(Mo))_3Si$ phase was the primary phase in both alloys. Whereas, the XRD and microstructural observation revealed that the Nb–19Si–3Mo alloy consisted of three phases of Nb_{ss}, $(Nb(Mo))_3Si$, and β-$(Nb,Mo)_5Si_3$. The primary phase in Nb–19Si–3Mo was β-$(Nb,Mo)_5Si_3$ rather than $(Nb(Mo))_3Si$. These suggest that the compositions of Nb–19Si–1 ~ 2Mo locate in $(Nb(Mo))_3Si$ region, while the Nb–19Si–3Mo is out of this region and near the second transition reaction (A detailed microstructural description for the Nb–19Si–3Mo alloy will be given in Section 4.1.5). The primary $(Nb(Mo))_3Si$ phase field is small and the Mo solubility in Nb_3Si is limited.

Figure 4 is a typical microstructure of Nb–19Si–2Mo. This microstructure consists of primary $(Nb(Mo))_3Si$ particles and a fine eutectic $(Nb(Mo))_3Si$–Nb_{ss} matrix. The primary $(Nb(Mo))_3Si$ shows angular block morphology. The morphology of primary $(Nb(Mo))_3Si$ phase is distinctly different from that of peritectic $(Nb(Mo))_3Si$ observed in Nb–20Si–1Mo (see Fig. 3(a)). The reason is not clear at present. The mean composition of $(Nb(Mo))_3Si$ dendrites is Nb–26.2Si–0.8Mo. The Si concentration is slightly higher than the stoichiometric composition.

4.1.4 $(Mo(Nb))_3Si$-region

Although no composition corresponding to $(Mo(Nb))_3Si$ was obtained in this study, there is clear evidence to the existence of this region. In Mo–Si phase diagram, the Mo_3Si-rich compositions locate between the eutectic (Mo_3Si–Mo_5Si_3) composition and the liquid composition of the L + Mo_{ss} → Mo_3Si peritectic. In Nb–Mo–Si system, the $(Mo(Nb))_3Si$-rich region must locate between the L + Nb_{ss} → $(Mo(Nb))_3Si$ peritectic ridge and the β-$(Nb,Mo)_5Si_3$–$(Mo(Nb))_3Si$ eutectic groove. The microstructural evidences for the existence of the L + Nb_{ss} → $(Mo(Nb))_3Si$ peritectic reaction and the β-$(Nb,Mo)_5Si_3$–$(Mo(Nb))_3Si$ eutectic reaction have been described in Sections 4.1.1 and 4.1.2.

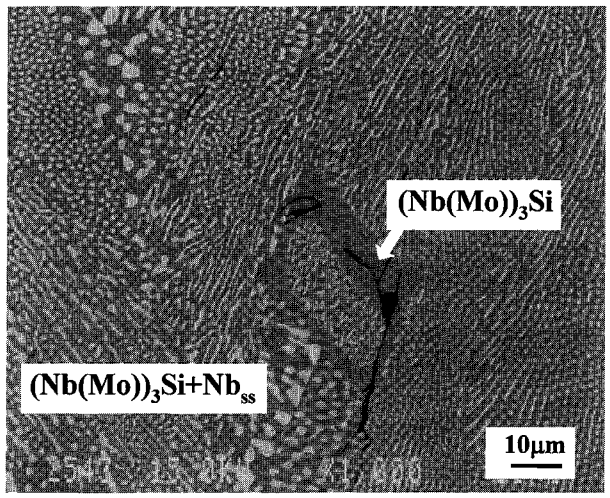

Fig. 4 BEI micrograph of Nb–19Si–2Mo alloy consisting of primary $(Nb(Mo))_3Si$ and eutectic of $(Nb(Mo))_3Si$–Nb_{ss}.

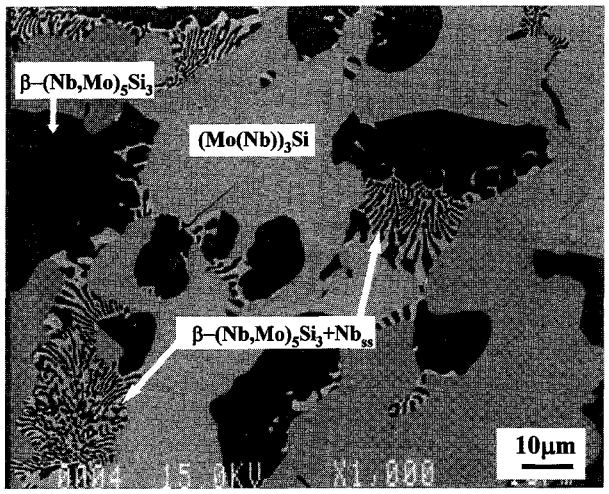

Fig. 5 BEI micrographs of Nb–25Si–50Mo alloy consisting of dark primary β-$(Nb,Mo)_5Si_3$ dendrites, large gray $(Mo(Nb))_3Si$ particles, and eutectic β-$(Nb,Mo)_5Si_3$–Nb_{ss}.

4.1.5 Compositions near the two transition reactions

Nb–25Si–50Mo: This composition was investigated to examine the first transition reaction of L + $(Mo(Nb))_3Si$ → β-$(Nb,Mo)_5Si_3$ + Nb_{ss}. Figure 5 shows the microstructure of Nb–25Si–50Mo alloy in the as cast condition. This BEI image revealed three constituent phases of β-$(Nb,Mo)_5Si_3$, $(Mo(Nb))_3Si$ and Nb_{ss}. The dark nonfaceted particles are β-$(Nb,Mo)_5Si_3$; the large, gray contrast phase is $(Mo(Nb))_3Si$; while the lamellar-like structure, which probably generated

from the final liquid to solidify at some inter-particle areas consists of β-$(Nb, Mo)_5Si_3$ (dark) and Nb_{ss} (light) phases. A small fraction of very fine Nb_{ss} particles is also observed at the edge regions of some large β-$(Nb, Mo)_5Si_3$ particles.

Since the dark nonfaceted β-$(Nb, Mo)_5Si_3$ particles are primary phase, the composition Nb–25Si–50Mo is suggested to locate in the primary β-$(Nb, Mo)_5Si_3$ phase field. The presence of the $(Mo(Nb))_3Si$ phase suggests the composition is near the eutectic β-$(Nb, Mo)_5Si_3$–$(Mo(Nb))_3Si$ groove. During solidification, the liquid meets it and results in formation of the eutectic β-$(Nb, Mo)_5Si_3$–$(Mo(Nb))_3Si$. However, the present $(Mo(Nb))_3Si$ phase is not a typical eutectic morphology, as described in Section 4.1.2 (see Fig. 3(c)). The reason remains unclear. The existence of the lamellar eutectic phase of β-$(Nb, Mo)_5Si_3$–Nb_{ss} suggests that the liquid reached the first transition reaction point, where the reaction of $L + (Mo(Nb))_3Si \rightarrow \beta$-$(Nb, Mo)_5Si_3 + Nb_{ss}$ occurred. However, we can not rule out the possibility that this transition reaction was suppressed due to the high cooling rate in the arc melting process. The final liquid reached the eutectic β-$(Nb, Mo)_5Si_3$–Nb_{ss} groove and led to the formation of the lamellar eutectic β-$(Nb, Mo)_5Si_3$–Nb_{ss}. Nevertheless, the first transition reaction must exist with a composition near Nb–25Si–50Mo.

Nb–19Si–3Mo: In Section 4.1.3, it has been indicated that the Nb–19Si–3Mo composition locates in the primary β-$(Nb, Mo)_5Si_3$ phase field and near the second transition reaction. Here, we will describe the microstructure in detail and examine the transition reaction of $L + \beta$-$(Nb, Mo)_5Si_3 \rightarrow (Nb(Mo))_3Si + Nb_{ss}$. Figure 6(a) shows the BEI image of this alloy at a low magnification. It contains two regions, which are distinguished by the contrast of gray and dark. The gray region is near the upper area of the ingot and the dark region near the bottom. Figures 6(b) and (c) show the enlarged views of these two areas. The gray region consists of large volume of fine-scale two-phase eutectic of $(Nb(Mo))_3Si$–Nb_{ss}, which is similar to the eutectic shown in Fig. 2(a). In the dark area, a few isolated, faceted, primary β-$(Nb, Mo)_5Si_3$ scatter in a fine-scale lamellar-like eutectic β-$(Nb, Mo)_5Si_3$–Nb_{ss} matrix. The mean composition of the block-shaped β-$(Nb, Mo)_5Si_3$ is Nb–38.6Si–0.8Mo.

The microstructure analysis suggests that the Nb–19Si–3Mo composition lies on the β-$(Nb, Mo)_5Si_3$-rich side of eutectic β-$(Nb, Mo)_5Si_3$–Nb_{ss} valley and near the second transition reaction. On the basis of the proposed diagram, a possible equilibrium solidification route can be described as follows:

1. $L \rightarrow \beta$-$(Nb, Mo)_5Si_3 + L$; followed by
2. $L \rightarrow \beta$-$(Nb, Mo)_5Si_3 + Nb_{ss} + L$; followed by
3. $L + \beta$-$(Nb, Mo)_5Si_3 \rightarrow (Nb(Mo))_3Si + Nb_{ss} + L$; then
4. $L \rightarrow (Nb(Mo))_3Si + Nb_{ss}$

It is not difficult to find the microstructural evidence of reaction 1 and 2. But the products of reaction 3 and 4 are same, the eutectic $(Nb(Mo))_3Si$–Nb_{ss}. It is note that the second transition reaction (3) is peritectic-type and would occur on the β-$(Nb, Mo)_5Si_3$ surface when the liquid composition reaches the transition reaction point. It is well known that the atoms transport process in a solid phase may be suppressed in a rapid cooling process. In the present case, the atom diffusion process might be suppressed partly due to a rapid cooling rate in

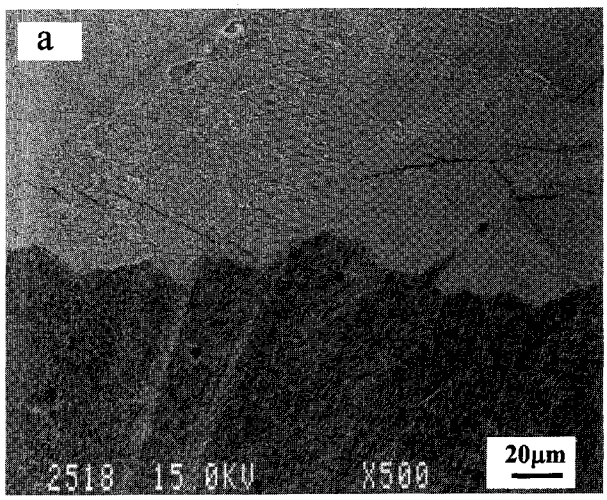

(a)

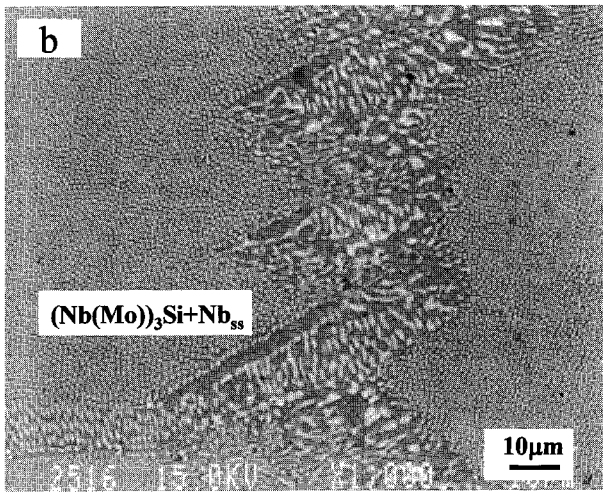

(b)

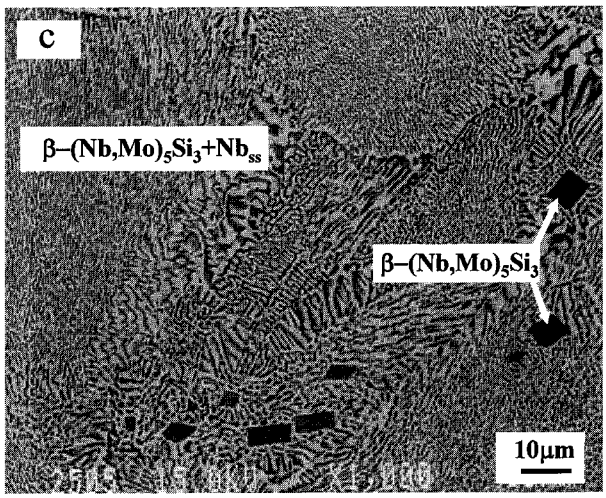

(c)

Fig. 6 BEI micrographs of Nb–19Si–3Mo showing (a) two different eutectic structures of (b) β-$(Nb, Mo)_5Si_3$–Nb_{ss} and (c) $(Nb(Mo))_3Si$–Nb_{ss}.

the arc melting process. Thus, reaction 3 might not be finished completely. It is therefore likely that the large volume fraction of eutectic $(Nb(Mo))_3Si$–Nb_{ss} phase is produced by the eutectic reaction (4) $L \rightarrow (Nb(Mo))_3Si + Nb_{ss}$ rather than the transition reaction.

4.2 Isothermal section at 1973 K

The phase equilibria at 1973 K were investigated for the ternary Nb–Mo–Si alloys heated to 1973 K and hold for 48 h. A brief description of these obtained results which are summarized in Fig. 7. In this diagram, the solid circles indicate the nominal alloy compositions, the open circles are the phase compositions, with the dashed lines as tie lines. The partial phase diagram contains four two-phase regions, namely, (1) α-$(Nb(Mo))_5Si_3 + Nb_{ss}$, (2) β-$(Nb,Mo)_5Si_3 + Nb_{ss}$, (3) $(Mo(Nb))_3Si + Nb_{ss}$, and (4) β-$(Nb,Mo)_5Si_3 + (Mo(Nb))_3Si$, and two three-phase regions, namely (1) α-$(Nb(Mo))_5Si_3 + \beta$-$(Nb,Mo)_5Si_3 + Nb_{ss}$ and (2) β-$(Nb,Mo)_5Si_3 + (Mo(Nb))_3Si + Nb_{ss}$. Though no compositions in the α-$(Nb(Mo))_5Si_3 + \beta$-$(Nb,Mo)_5Si_3 + Nb_{ss}$ three-phase region were studied in this work, the XRD and EPMA results revealed that the silicide phase in Nb–16Si–15Mo alloy is α-$(Nb(Mo))_5Si_3$ with a composition of Nb–38.5Si–1.5Mo, while the silicide in Nb–16Si–20Mo alloy is β-$(Nb,Mo)_5Si_3$ with a composition of Nb–38.5Si–3.1Mo. Thus, a three-phase region of β-$(Nb,Mo)_5Si_3 + \alpha$-$(Nb(Mo))_5Si_3 + Nb_{ss}$ must exist between the two tie lines through the compositions of Nb–16Si–15Mo and Nb–16Si–20Mo, receptively. The α-$(Nb(Mo))_5Si_3$ region is very small and the maximum solubility of Mo in α-$(Nb(Mo))_5Si_3$ phase is estimated to be ~1.5%. For the alloy of Nb–25Si–50Mo, the XRD results revealed three phases of Nb_{ss}, β-$(Nb,Mo)_5Si_3$ and $(Mo(Nb))_3Si$, suggesting a equilibrium relationship among these three phases at 1973 K. EPMA results revealed the compositions of these phases to be Nb–22.2Mo–1.9Si for Nb_{ss}, Nb–33.2Mo–38.5Si for β-$(Nb,Mo)_5Si_3$, and Nb–23.6Mo–24.9Si for $(Mo(Nb))_3Si$, respectively. The three-phase field is determined from these compositions of the three phases. The Nb solubility in $(Mo(Nb))_3Si$ is ~23.6%.

5. Conclusions

Four phases exist in the as-cast ternary Nb–Mo–Si alloys lie in the Nb–Mo-rich zone: β-$(Nb,Mo)_5Si_3$, $(Nb(Mo))_3Si$, $(Mo(Nb))_3Si$, and Nb_{ss}. The phases observed were dendritic, peritectic, or eutectic in nature, depending on the composition and solidification path. In the partial liquidus surface projection, there are two transition reactions of $L + (Mo(Nb))_3Si \rightarrow \beta$-$(Mo(Nb))_5Si_3 + Nb_{ss}$ and $L + \beta$-$(Nb,Mo)_5Si_3 \rightarrow (Nb(Mo))_3Si + Nb_{ss}$. The first transition reaction occurs at a composition near Nb–25Si–50Mo and the second near Nb–19Si–3Mo. The eutectic and peritectic reactions included in this partial diagram are summarized as follows:

$$L \rightarrow \beta\text{-}(Nb,Mo)_5Si_3 + (Mo(Nb))_3Si$$

$$L + Nb_{ss} \rightarrow (Mo(Nb))_3Si$$

$$L \rightarrow \beta\text{-}(Nb,Mo)_5Si_3 + Nb_{ss}$$

$$L + \beta\text{-}(Nb,Mo)_5Si_3 \rightarrow (Nb(Mo))_3Si$$

$$L \rightarrow (Nb(Mo))_3Si + Nb_{ss}$$

The most important feature of this diagram is the existence of the eutectic reaction of $L \rightarrow \beta$-$(Nb,Mo)_5Si_3 + Nb_{ss}$. The lamellar nature of the eutectic β-$(Nb,Mo)_5Si_3 + Nb_{ss}$ is helpful to produce Nb/Nb silicide *in-situ* composites with refined silicide microstructure.

A partial isothermal section of Nb–Mo–Si ternary system at 1973 K has been proposed. This phase diagram contains four equilibrium two-phase fields of (1) α-$(Nb(Mo))_5Si_3 + Nb_{ss}$, (2) β-$(Nb,Mo)_5Si_3 + Nb_{ss}$, (3) $(Mo(Nb))_3Si + Nb_{ss}$, and (4) β-$(Nb,Mo)_5Si_3 + (Mo(Nb))_3Si$, and two equilibrium three-phase fields of (1) α-$(Nb(Mo))_5Si_3 + \beta$-$(Nb,Mo)_5Si_3 + Nb_{ss}$ and (2) β-$(Nb,Mo)_5Si_3 + (Mo(Nb))_3Si + Nb_{ss}$. The solubility of Mo in α-$(Nb(Mo))_5Si_3$ phase is estimated to be ~1.5%, and the Nb solubility in $(Mo(Nb))_3Si$ is ~23.6%.

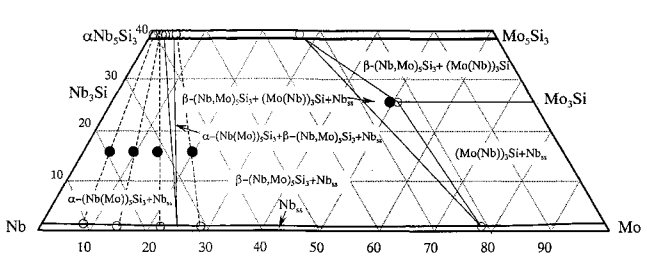

Fig. 7 An isothermal section diagram of Nb–Mo–Si ternary system at 1973 K. The nominal compositions of tested alloys are shown as solid circles and the phase compositions measured by EPMA are shown as open circles.

Acknowledgements

This research was supported by a grant from the New Energy and Industrial Technology Development Organization (NEDO) of Japan.

REFERENCES

1) B. P. Bewlay, J. J. Lewandowski and M. R. Jackson: JOM, **49**(8) (1997), 44–45.
2) M. R. Jackson, B. P. Bewlay, R. G. Rowe, D. W. Skelly and H. A. Lipsitt: JOM, **48**(1) (1996), 39–44.
3) P. R. Subramanian, M. G. Mendiratta and D. M. Dimiduk: JOM, **48**(1) (1996), 33–38.
4) S. Hanada: *Reports of the 123 committee on Heat-Resisting Metals and Alloys*, JSPS, **38** (1997), pp.299–307.
5) R. T. Begley: *Evolution of Refractory Metals and Alloys*, ed. by E. N. C. Dalder, T. Grobstein and C. S. Olsen: The Minerals, Metals & Materials Society (TMS), Warrendale, (1994), pp. 29–48.
6) C. L. Ma, H. Tanaka, Y. Tan, A. Kasama, R. Tanaka, Y. Mishima and S. Hanada: Collected Abstracts of the 1999 Autumn Meeting of the Japan Institute of Metals, (1999), pp. 310.
7) D. M. Shah and D. L. Anton: *Intermetallic Matrix Composites II*, ed. by D. B. Miracle, D. L. Anton, J. A. Graves: Mater. Res. Soc. Symp. Proc. Vol. 273, Pittsburgh, PA (1992), pp. 385–397.
8) Dilip M. Shah, Donadl L. Anton, David P. Pope and Stephen Chin: Mater. Sci. & Eng. A, **192/193** (1995), 658–672.
9) T. B. Massalski, H. Okamoto, P. R. Subramanian and L. Kacprzak: *Binary Alloy Phase Diagrams*, ASM, Metals Park, Ohio, (1992).

10) C. L. Ma, A. Kasama, H. Tanaka, Y. Tan, R. Tanaka, Y. Mishima and S. Hanada: Mater. Trans., JIM, **41**(6) (2000), 719–726.
11) M. G. Mendiratta, J. J. Lewandowski and D. M. Dimiduk: Metall. Trans. A, **22A** (1991), 1573–1583.
12) B. P. Bewlay, M. R. Jackson and H. A. Lipsitt: Journal of Phase Equilibria, **18**(3) (1997), 264–278.
13) M. G. Mendiratta and D. M. Dimiduk: *in High-Temperature Ordered Intermetallic Alloys III*, ed. by C. T. Liu, A. I. Taub, N. S. Stoloff and C. C. Koch: Mater. Res. Soc. Proc. Vol. 133, Pittsburgh, PA (1989), pp. 441–446.